Research article

Synthesizing covalent organic frameworks for unprecedented iodine capture performance☆

Shaikha S. AlNeyadi [a],[*], Mohammed T. Alhassani [b], Ali S. Aleissaee [a], Sultan. J [a], Abdullah H. Khalaf [a], Abdulrahman A. Alteneij [a], Yaser Y. Alyaarbi [a]

[a] Department of Chemistry College of Science, UAE University Al-Ain, 15551, United Arab Emirates
[b] Department of Chemical Engineering, College of Engineering, Al Ain, 15551, United Arab Emirates

ABSTRACT

Nuclear energy continues to be an important supplier of electricity, but it has problems with waste management and the possibility to leak radioactive material. Iodine, a potentially harmful byproduct of uranium fission, is hazardous to both the environment and human health. Therefore, developing safe, effective, and affordable storage facilities for iodine waste is crucial. Owing to their well-controlled pore structure and substantial certain surface area, covalent organic frameworks (COFs) show promise for the adsorption of radioactive iodine. The newly developed COFs (SJ-COF, YA-COF, and AA-COF) shown amazing properties, including strong thermal and chemical stability, which made them ideal for efficient iodine capture. Notably, the ultrahigh iodine capture capacities of these COFs—8.52 g g^{-1}, 8.12 g g^{-1} and 7.01 g g^{-1}—were significantly greater than most previously reported materials. And The % removal efficiency for SJ-COF, YA-COF and AA-COF from I$_2$/cyclohexane solutions were 87.9 %, 88.6% and 82.6 % respectively. It is noteworthy that the three COFs have high selectivity, reusability, and iodine retention abilities, maintaining iodine even after five recyclings. Based on the outcomes of the experiments, the adsorption processes of the three COFs were examined, and it was discovered that iodine was bound through physical-chemical adsorption. The findings of our work provide a groundbreaking standard for the removal of nuclear waste and demonstrate the enormous potential of COFs as adaptable porous structures that may be specifically designed to address major environmental concerns.

1. Introduction

Nuclear energy is a pivotal alternative to fossil fuels, offering a higher energy density and significantly lower emissions of CO$_2$, SO$_x$, NO$_x$, and particulate matter, thus representing a more ecologically sustainable option at the point of use. In 2020, 440 nuclear power reactors globally accounted for 10% of the world's electricity generation, with expectations of substantial growth over the next decade [1–3]. However, the management of radioactive waste, particularly volatile radionuclides such as iodine-129 and iodine-131, presents a significant challenge. These isotopes pose serious risks to human health and the environment due to their long half-lives and high mobility [1,4,5]. Historical nuclear accidents, such as those at Three Mile Island, Chernobyl, and Fukushima, highlight the urgent need

---

Scheme 1. Designing and Synthesizing SJ-COF, YA-COF, and AA-COF.

for effective radioactive waste management strategies [2,4]. Traditional inorganic adsorbents for radioactive iodine, like zeolites and Ag-doped silica, are limited by cost, efficiency, and stability issues in humid environments [6]. Recent advancements have focused on alternative materials, including carbon-based adsorbents, algae, and modified bagasse, for their potential in pollutant removal due to their cost-effectiveness and high adsorption capacities [7–9]. Efforts to address iodine contamination have spurred the investigation of various materials and methods. Notably, cost-effective adsorbents like rice husks, coconut shells, sawdust, bentonite, and zeolites have been repurposed for environmental clean-up. Concurrently, methods such as ozonation, oxidative techniques, ion exchange, and adsorption have been assessed for their iodine removal efficacy. Each approach has its merits and drawbacks: ozonation may not ensure complete pollutant removal and risks byproduct formation [10], while oxidative techniques need optimization for radioactive iodine [11]. Ion exchange offers ion replacement but struggles with selectivity and longevity [3,12]. This exploration underscores the diverse strategies in mitigating iodine pollution, emphasizing the necessity for efficient and sustainable solutions.

Despite the variety of available methods, the adsorption technique stands out for its simplicity, ease of operation, and high efficiency, making it a focal point of current research efforts. Metal-organic frameworks (MOFs) and porous organic polymers (POPs), including covalent organic frameworks (COFs), have shown great promise in iodine capture due to their vast surface areas and stability. MOFs, despite their potential, are limited by low stability in high temperatures and aqueous environments [13]. In contrast, POPs—comprising COFs, conjugated microporous polymers, porous aromatic frameworks, and hypercrosslinked polymers—benefit from robust covalent bonds, offering enhanced stability [14]. COFs, in particular, stand out for their covalent bonds, crystalline structure, and adjustable porosity, contributing to their superior iodine adsorption capability. Their notable features include high stability, organized channel structures, and large surface areas, akin to MOFs, but with added benefits like low density and functional versatility [16]. This makes COFs highly effective for various applications beyond iodine capture, such as gas storage, catalysis, and semiconduction. Recent studies highlight COFs' exceptional performance in trapping iodine from fission reactor waste, with notable examples like TFB-DB COF and COF-DL229 demonstrating significant gravimetric porosities [15,16]. Recent studies underline the critical role of COFs in environmental remediation, offering groundbreaking insights into their applications in capturing volatile pollutants [17,18]. This work builds on these advancements, positioning COFs at the forefront of research on sustainable methods for managing radioactive contaminants. This study addresses the environmental and health hazards posed by the disposal of radioactive iodine, a byproduct of uranium fission. It introduces covalent organic frameworks (COFs) as innovative adsorbents for radioactive iodine, focusing on specific COFs (SJ-COF, YA-COF, and AA-COF) synthesized through Schiff base reactions. These COFs, featuring rich heteroatoms, extended π-conjugations, and abundant pore structures, demonstrate superior stability and efficiency in iodine capture, both in vapor and in cyclohexane solution, with removal efficiencies between 82.6% and 88.6% and vapor adsorption capacities up to 8.52 g g^{-1}. Their high selectivity, reusability, and retention abilities after multiple recycling processes underscore their potential for long-term radioactive iodine management. The study also explores the adsorption mechanisms, highlighting the role of physical-chemical interactions and the synergistic effects of TTF and TPE-based COFs in enhancing iodine capture through a combination of physical adsorption and chemisorption. Overall, this study explores into the efficient capture of hazardous iodine using COFs, investigating the structural framework's relationship with their adsorption performance.

2. Results and discussion

Designing COFs with very effective iodine absorption capacity depends critically on selecting the right linkers. For improving iodine adsorption, linkers that permit the production of large and uninterrupted conjugated π-systems as well as the insertion of electron-rich groups suchlike –NH–, –NH$_2$, –C=N-, aromatic system, tetrathiafulvalene, and heterocycles moieties, are particularly desired. These electron-rich groups promote the development of charge-transfer complexes with electron-deficient I$_2$, which enhances the contact and affinity between the COF and iodine as well as the capacity and rate of adsorption [19,20]. We designed and created three COFs with outstanding stability and porosity by Schiff base reactions, as shown in Scheme 1, to accomplish significant iodine sorption capacity. We presented a TTF-based group called tetrathiafulvalene-tetrabenzaldehyde (TTF-TBA, Scheme 1A) as a 4-connected planar construction block (as aldehyde linker). Radical cations are known to arise when TTF-based derivatives interact aggressively with electron acceptors such I$_2$ [15]. We anticipated that adding TTF-based units to the COF materials will improve iodine adsorption through this powerful connection. In our design, we employed 4,7-diaminobenzo [c] [1,2,5]thiadiazole (DABTH, Scheme 1A) as a linear building unit and 1,3,6,8-tetra (aminophenyl)pyrene (TAPA, Scheme 1B) as a 4-connected building unit, functioning as amine linkers. Due to the condensation of TTF-TBA with linear DABTH and 4-connected TAPA, respectively, two structures—the two-dimensional (2D) SJ-COF and YA-COF—were created. In addition, AA-COF was produced as Yellow crystals by solvothermal reaction of 4,4′,4″,4‴-(ethane-1,1,2,2-tetrayl)tetra benzaldehyde (ETBA) (ETBA, Scheme 1C) with hydrazine. The details of organic linkers synthesis methods, including reagents, reaction conditions, and purification techniques. Additionally, comprehensive characterization techniques, such as spectroscopic analysis (e.g., NMR) are included in the supporting data (SI, Section S2, Scheme S1-S4 and Section 3, Figs. S1–S8). A solvothermal technique was used to create the three targeted COFs. Acetic acid was used as a catalyst and the building blocks were suspended in a solution composed of a mixture of (mesitylene/1,4-dioxane) or *o*-(dichlorobenzene/*n*-butanol) and exposed to solvothermal conditions at 120 °C for three days (SI, Section S4). The successful creation of imine bonds was shown by the FT-IR spectroscopy study of SJ-COF, YA-COF, and AA-COF, which showed strong stretching vibrations of the C=N unit in the range of 1619–1626 cm^{-1}. Further evidence of the success of the Schiff-base condensation process was provided by the spectra, which also revealed the removal of the N–H (3437 and 3350 cm^{-1}) stretching vibrations from the amino group in the amine linker and the C=O (1648 cm^{-1}) vibration from the aldehyde linker (SI, Section S5, Fig. S9). For COFs to be used in practical applications, stability is essential. In our research, we successfully synthesized SJ-COF, YA-COF, and AA-COF and looked into their chemical and thermal stability. The findings showed that these COFs had extraordinary stability, making them very attractive materials for uses requiring
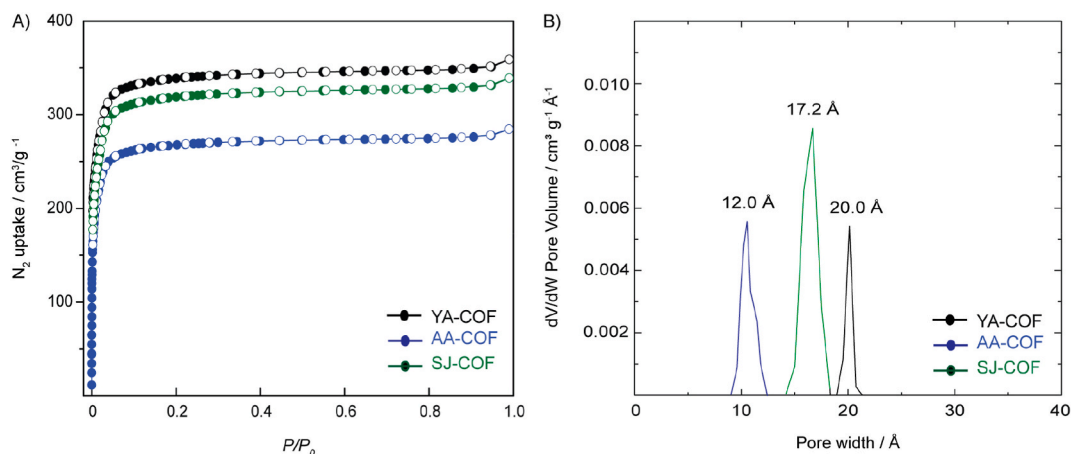
Fig. 1. A) Nitrogen sorption isotherms of YA-COF, AA-COF and SJ-COF, at 77 K, with ● representing adsorption and ○ representing desorption. Samples were pre-treated by degassing at 100 °C for 12 h. The profiles, exhibiting type I isotherms with microporous structures; B) Pore size distributions of YA-COF, AA-COF and SJ-COF determined through Nonlocal Density Functional Theory (NLDFT) from the adsorption data, highlighting the uniform and specific pore sizes of each COF, showcasing the uniformity and primary pore sizes of each COF, essential for selective adsorption applications.
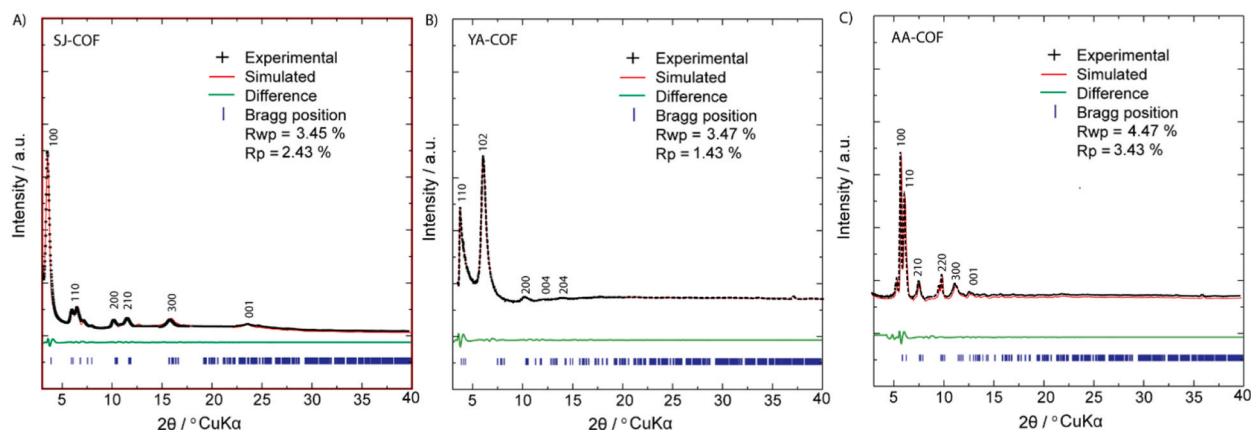
Fig. 2. PXRD analysis of SJ-COF, YA-COF, and AA-COF: Experimental data (black dashed lines), Pawley refinement (red lines), Bragg positions (blue lines), and difference plots (green lines) illustrate structure accuracy and crystallinity.

resistance to chemical reactions and high temperatures. The COFs had outstanding thermal stability, as measured by thermogravimetric analysis (TGA), since they maintained their structural integrity even at high temperatures without significantly losing weight or decomposing. Notably, these COFs did not start to break down until they reached 400 °C in a nitrogen environment. Additionally, we tested the chemical stability of the SJ-COF, YA-COF, and AA-COF samples over a 24-h period at room temperature in a variety of solvents, including boiling water, ethanol, N,N-dimethylformamide, dimethylsulfoxide, 3 M HCl at 25 °C, and 3 M NaOH at 25 °C. Surprisingly, following this procedure, the PXRD patterns of the SJ-COF, YA-COF, and AA-COF samples remained robust and in their initial positions, demonstrating that the remarkable crystallinity of these COFs can be successfully maintained even under difficult circumstances (SI, Section S5, Figs S10-S12). These findings confirm the good chemical stability of SJ-COF, YA-COF, and AA-COF, which makes them suitable candidates for functionalization. The COFs' attractiveness as chemically and thermally stable materials is further boosted by their crystalline structure, and porous features. Using nitrogen sorption isotherms at 77 K, the porous architectures of SJ-COF, YA-COF, and AA-COF were examined (Fig. 1). The COF samples received overnight pre-treatment at 100 °C in vacuum prior to the nitrogen sorption measurement. The nitrogen absorption of SJ-COF, YA-COF, and AA-COF increased quickly at lower pressures ($P/P_0 = 0$ to 0.1), demonstrating their microporous characteristics. SJ-COF, YA-COF, and AA-COF were found to have 870 $m^2\,g^{-1}$, 1098 $m^2\,g^{-1}$, and 620 $m^2\,g^{-1}$ of Brunauer-Emmett-Teller (BET) surface area, respectively. At $P/P_0 = 0.99$, which was used to compare the three COFs' total pore volumes, The YA-COF showcased an impressive pore volume of 1.22 $cm^3\,g^{-1}$, outperforming the SJ-COF and AA-COF, which had pore volumes of 0.93 $cm^3\,g^{-1}$ and 0.98 $cm^3\,g^{-1}$, respectively. The pore sizes of SJ-COF, YA-COF, and AA-COF were computed using the nonlocal density functional theory (NLDFT) and were found to be 12 Å, 17.2 Å, and 20 Å, respectively.
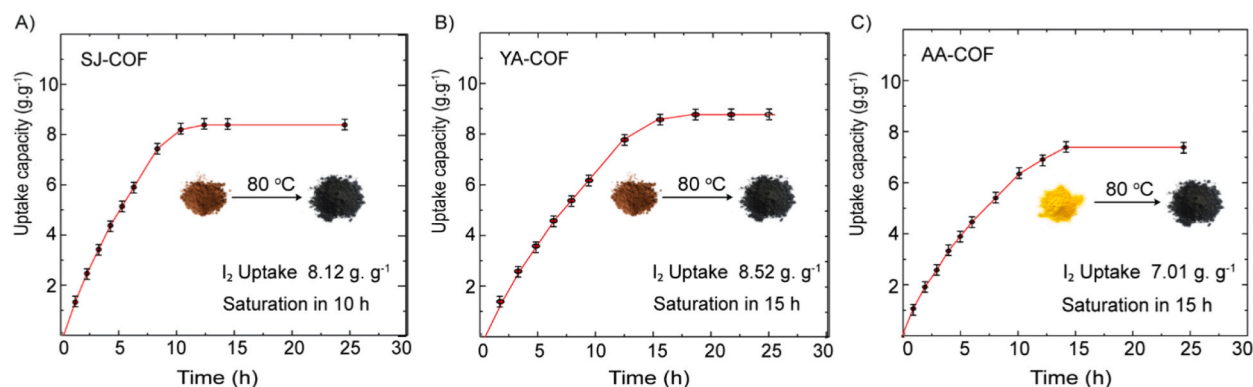
Fig. 3. Gravimetric iodine uptake of SJ-COF, YA-COF, and AA-COF varies over time at 80 °C and under ambient pressure conditions. Iodine vapor exposure was consistent across samples in a sealed environment, with uptake monitored over time to assess adsorption kinetics. Error bars indicate standard deviations from three parallel experiments, affirming data reliability. This experiment underscores the COFs' efficacy in gas capture, evident from their iodine uptake capabilities.

The crystallinity characteristics of SJ-COF, YA-COF, and AA-COF were examined using a powder X-ray diffraction (PXRD) study (Fig. 2). Six different peaks were seen for SJ-COF (Fig. 2A), each representing the 100, 110, 200, 210, 300, and 001 facets. They were found at 4.06°, 6.93°, 10.89°, 12.05°, 16.34°, and 24.06°. Similar to this, YA-COF (Fig. 2B) showed five peaks at 2.68°, 5.58°, along with others at 9.82°, 11.54°, and 15.35°, which were attributed to the 110, 102, 200, 004, and 204 facets, respectively. Regarding AA-COF (Fig. 2C), six distinct peaks were seen, with the peak with the highest intensity being at 5.58°. The other peaks were at 6.98°, 7.32°, 9.62°, 11.24°, and 13.88°, and they corresponded to the 100, 110, 210, 220, 300, and 001 facets, respectively The powder X-ray diffraction (PXRD) patterns of the analyzed COFs were simulated using the Pawley refinement approach to acquire a fuller knowledge of their structures. The simulated PXRD patterns (Fig. 2A–C, red curve) closely resemble the experimental PXRD patterns (Fig. 2A–C, black curve), as evidenced by the difference pattern (Fig. 2A–C, green curve). For SJ-COF (Fig. 2A), the experimental PXRD pattern aligned well with the simulated patterns obtained from the AA-staggered stacking model, showing good agreement factors (Rp = 2.43% and Rwp = 3.45%) with the optimized parameters (a = b = 19.86 Å, c = 3.54 Å, α = β = 90°, and γ = 120°). For YA-COF, the cell parameters were optimized using the Pawley refinements, and there was little difference between the experimental curve and the simulated profiles produced by the AA-staggered stacking model (a = b = 30.13 Å, c = 3.50 Å, α = β = 90°, and γ = 120°) was negligible (Rp = 1.43% and Rwp = 3.47%) (Fig. 2B). Additionally, the experimental patterns and the XRD pattern generated from the AA-eclipsed stacking models of AA-COF (Fig. 2C) were in excellent agreement. On the other hand, the pattern derived from their corresponding AB' staggered stacking model significantly deviated from the experimental results. The refined unit cell of AA-COF is a = 21.22 Å, b = 21.21 Å, and c = 4.40 Å with α = β = γ = 90° (residuals Rwp = 4.47% and Rp = 3.43%) (SI, Section S5, Fig. S13).

3. Iodine uptake experiment

Gas-phase. The design and building of large π—π-conjugated systems can be used to create COF materials with strong iodine absorption characteristics. Incorporating electron-rich groups like –C=N-, –OCH$_3$, aromatic rings, tetrathiafulvalene, and heterocycles is one possible strategy. The development of charge-transfer complexes is made possible by these additions, increasing the adsorption capacity and rate. Furthermore, the total iodine capture efficiency of functional group-modified COF absorbers is significantly enhanced by this adjustment of the adsorption-driving force between them. The potential of this approach lies in the ability to create COF materials with exceptional iodine uptake capabilities. Given the ongoing rise in iodine pollution in nuclear waste, SJ-COF, YA-COF, and AA-COF were employed to capture iodine vapor. These synthetic COFs are very rich in sulfur and nitrogen atoms, which makes them excellent in adsorbing iodine. The three activated COFs (SJ-COF, YA-COF, and AA-COF) were evaluated for gaseous iodine absorption capability utilizing triple parallel tests at varied time intervals. These COF samples were subjected to an iodine adsorption experiment that involved iodine vapor at a temperature of 80 °C and at standard atmospheric pressure. To ascertain the iodine intake, gravimetric measurements were taken at various time intervals. The iodine uptake patterns of the three COFs (SJ-COF, YA-COF, and AA-COF) throughout a 27-h period are shown in Fig. 3. The sample weights for SJ-COF, YA-COF, and AA-COF increased significantly during each period of time. Notably, the iodine absorption in all three COFs was quick, with adsorption saturation being reached in 10 h for SJ-COF, 15 h for YA-COF, and 15 h for AA-COF (Fig. 3). Iodine uptakes were shown in AA-COF to be as high as 7.01 g g^{-1}, SJ-COF to be as high as 8.12 g g^{-1}, and YA-COF to be noticeably higher at 8.52 g g^{-1}. The inset photos in Fig. 3A, B, and 3C show an interesting color shift following the end of the adsorption process. Further proof of iodine absorption may be seen in the transformation of AA-COF from light yellow, SJ-COF and YA-COF from brown to dark black. In our study, we synthesized three distinct covalent organic frameworks (COFs) as potential adsorbents for iodine capture: tetrathiafulvalene (TTF)-based COFs represented by SJ-COF and YA-COF, and a tetraphenylethene (TPE)-based COF, AA-COF. Our research aimed to investigate the relationship between the COF structures and their iodine uptake capabilities.

Role of Functional Groups: In summary, YA-COF's exceptional iodine capture performance (8.52 g g^{-1}) can be attributed to the
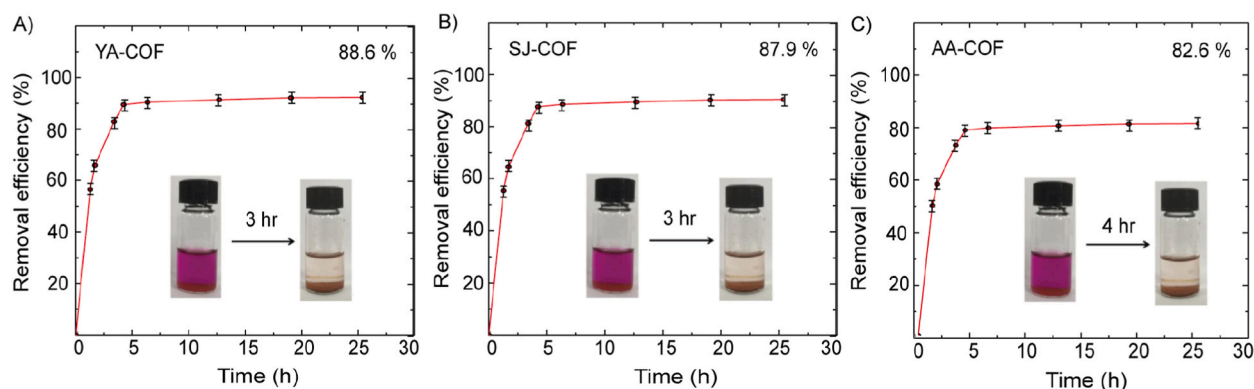
Fig. 4. Iodine Removal Efficiency of COFs in Cyclohexane Solution. Removal efficiency curve of iodine by YA-COF, SJ-COF and AA-COF in various times in cyclohexane solution (300 mg L^{-1}) during 24 h; The inset images show the gradual color change from purple to colourless by immersing COFs composite in I$_2$/cyclohexane solution. Error bars denote standard deviations from three replicates, ensuring result reliability. This highlights COFs' applicability in pollutant adsorption.

strategic incorporation of Tetrathiafulvalene (TTF) and pyrene groups within its structure. Tetrathiafulvalene (TTF) groups incorporated into YA-COF play a crucial role in enhancing its iodine capture capabilities. TTF is known for its electron-donating properties, facilitating charge transfer interactions with iodine molecules. Within YA-COF, these TTF groups readily donate electrons to iodine atoms, forming charge transfer complexes. This chemical interaction significantly increases YA-COF's affinity for iodine. The electron-donating nature of TTF not only promotes chemical bonding with iodine but also boosts YA-COF's overall iodine uptake capacity, making it highly effective in capturing iodine gas. The introduction of pyrene groups into YA-COF enhances its iodine capture capabilities through π-π stacking interactions. Pyrene, known for its fused aromatic ring structure, provides a unique platform for these interactions. In the context of iodine capture, where iodine molecules are held together by weak van der Waals forces and possess π electrons, the aromatic rings of pyrene are well-suited for π-π stacking. This physical adsorption mechanism complements the chemical interactions facilitated by the Tetrathiafulvalene (TTF) groups in YA-COF, collectively boosting its ability to capture iodine. In essence, the synergy between chemical bonding (TTF groups) and physical adsorption (pyrene groups) within YA-COF significantly enhances its iodine capture efficiency. This combination of functionalities underscores the material's effectiveness in capturing iodine gas, making it a promising adsorbent for such applications.

Pore Structure and Surface Area: The differences in iodine uptake can also be linked to variations in the pore structure and surface area of these COFs. YA-COF, with its specific pore dimensions and high surface area (1098 m^2 g^{-1}) with a remarkable pore volume of 1.22 cm^3 g^{-1}, provided ample space for iodine molecules to be adsorbed. The porous network within YA-COF likely facilitated physical adsorption. In summary, the observed variation in iodine uptake among SJ-COF, YA-COF, and AA-COF can be attributed to a combination of factors, including functional groups, pore structure, surface area, and conformational flexibility. YA-COF, with its specific functional groups and optimal pore structure, emerged as the most effective iodine adsorbent in our study. This underscores the importance of understanding the structure-activity relationship in designing COF-based materials for gas adsorption applications, such as iodine capture. Further investigations into the detailed interactions and structural features of these COFs can provide valuable insights for the design of highly efficient adsorbents for specific applications. When YA-COF is compared to previously reported materials, it has remarkable iodine absorption capabilities. It greatly exceeds other known materials with a high sorption capacity of 8.52 g g^{-1}. For instance, it uptakes iodine more efficiently than standard silver-doped zeolite mordenite (Ag-MOR) by 29 times (0.28 g g^{-1}) [21]. Furthermore, YA-COF's adsorption capacity is nearly two orders higher more than that of nonporous materials and far better than typical porous structures, comprising zeolitic imidazolate framework-8 (ZIF-8, 1.20 g g^{-1}) [22], porous aromatic framework (PAF-24, 2.76 g g^{-1}) [17], and azo-bridged porphyrin–phthalocyanine network (AzoPPN, 2.90 g g^{-1}) [23]. Moreover, it also has a certain competitiveness compared with other COFs with various pore volumes, surface areas, and pore diameters for iodine absorption as can be seen in (SI, Section S6, Table S1) making YA-COF attractive candidate in the field of iodine containment.

Liquid-phase. Due to their exceptional chemical and thermal stability, as well as their high porosity, the SJ-COF, YA-COF, and AA-COF materials have demonstrated tremendous potential as efficient water pollutants capture agents. we chose to quantitatively evaluate their capacity to adsorb iodine from a cyclohexane solution after being encouraged by their good performance in adsorbing iodine vapor. For this test, powdered samples of SJ-COF, YA-COF, and AA-COF were submerged for 24 h in a sealed vial of cyclohexane solution containing 300 mg L^{-1} iodine. Then, using UV–visible spectra to track changes in absorption intensity, the adsorption capacity was determined. The fact that the concentration of iodine decreased over time as shown in (SI, Section S7, Fig S14) suggests that the COFs successfully absorbed iodine. The pattern in the color shift is confirmed by the time-dependent UV–vis spectroscopy data, which demonstrates iodine absorption at 528 nm. The effectiveness of iodine removal was estimated and presented in Fig. 4. It was evident from the removal efficiency curve that the sorption of iodine by COFs experienced a significant increase within 3–4 h. Due to the significant iodine molecule occupancy of active sites on the sorbent, the resting time rate was extended to 24 h. After this time, the system gradually attained a stable equilibrium condition. Remarkably high removal efficiencies were achieved, with almost complete removal of iodine at approximately 87.9%, 88.6%, and 82.6% using only 10 mg of SJ-COF, YA-COF, and AA-COF adsorbents,

Table 1

Lists the parameters determined using various isotherm models.

	Pseudo first-order kinetic model	Pseudo second-order kinetic model
	K_1(1/h) Q_e(%) R^2	K_1 (1/h) Q_e (%) R^2
SJ-COF	0.06742 95.64 0.9168	8.41×10^{-4} 87.90 0.997
YA-COF	0.06303 92.95 0.9242	8.10×10^{-4} 88.60 0.990
AA-COF	0.06013 90.83 0.8923	7.14×10^{-4} 82.61 0.987

Table 2

Calculated parameters obtained using various models of adsorption kinetics.

	Langmuir model	Freundlich model
	Q_m (mg/g) k_L (1/mg) **R^2**	K_F(1/mg) n **R^2**
SJ-COF	960.15 0.0035 0.990	13.40 1.03 0.9628
YA-COF	895.20 0.0033 0.990	13.2 1.02 0.9721
AA-COF	768.43 0.0030 0.990	12.6 1.04 0.9753

respectively, in a 300 mg L^{-1} I$_2$/cyclohexane solution. The original purple-colored solution changed over time and became colorless. Simultaneously, the color of the COFs powder gradually changed from yellow or brown to black, demonstrating the efficiency with which SJ-COF, YA-COF, and AA-COF gathered iodine from the cyclohexane solution.

Pseudo-first-order and pseudo-second-order kinetic models were used to examine the experimental data in order to acquire a clearer understanding of the link between removal efficiency and time. Eqs. (1) and (2), which are linear representations of these models, are as follows:

$$ln(Q_e \; - \; Q_t\;) = ln \; Q_e \; - \; k_1 t \tag{1}$$

$$\frac{t}{Q_t} = \frac{1}{k_2 Q^2 e} + \frac{t}{Q_e} \tag{2}$$

Table 1 lists the kinetic parameters and corresponding coefficients for the pseudo-first-order and pseudo-second-order models of the adsorption process. The mass percent of iodine adsorbed at time t and equilibrium, respectively, are represented in these models by Q_t and Q_e. The pseudo-first-order rate constant of the adsorption process is denoted as k_1, with units of h^{-1}, while the pseudo-second-order rate constant is denoted as k_2, with units of (% h)$^{-1}$. The investigation showed a significant match of the adsorption kinetics to the pseudo-second-order model in contrast to the pseudo-first-order model, as demonstrated by large correlation coefficient (R^2) values of 0.997, 0.990, and 0.987 for SJ-COF, YA-COF, and AA-COF, respectively. These findings suggested that the pseudo-second-order kinetic model may adequately represent the existing adsorption system. The validity of this conclusion was further reinforced by examining the fitting curve of the pseudo-second-order kinetic model, as demonstrated in the Supplementary Information (SI, Section S7, Fig S15). The findings showed a strong connection between the molecules of the adsorbent and iodine, suggesting that the rate-controlling step is probably controlled by a chemical interaction mechanism. This finding emphasizes how the adsorbent and iodine form strong bonding and affinity interactions throughout the adsorption process [24].

The ability to calculate the saturated iodine adsorption capacity of COFs was made possible by the adsorption isotherm investigations, which were vital in understanding the interaction between COFs and iodine [25]. In the adsorption isotherm evaluations, where the starting iodine concentrations varied between 60 mg L^{-1} and 180 mg L^{-1}, the results are shown in (SI, Section S7, Fig S16). The figure shows that the equilibrium adsorption capacity first showed a linear climb, followed by a steady rise, as the initial concentration of the iodine solution rose. For the purpose of describing solid-liquid adsorption systems, the Langmuir and Freundlich adsorption isotherm models are both often utilized [25]. The Langmuir and Freundlich adsorption isotherm models were used to fit the isotherm curve in order to obtain further understanding of the interaction between COFs and iodine in aqueous solution. Eqs. (3) and (4) serve as representations of their linear forms.

$$Q_e = \frac{Q_m k_L C_e}{1 + k_L C_e} \tag{3}$$

$$Q_e = K_F \; C_e^{\;1/n} \tag{4}$$

In this study, C_e (mg/L) stands for the equilibrium iodine solution concentration, Q_m (mg/g) is the theoretical maximum adsorption value, k_L (L/mg) and K_F (mg/g) are the adsorption constants for the Langmuir and Freundlich isotherm models, respectively, and *n* is the Freundlich linearity index [26]. The computed values are represent in Table 2 after the experimental data were fitted using the Langmuir and Freundlich models. Comparing the two models, it was found that the Langmuir model offered a better match to the experimental findings with higher correlation coefficients (R^2 values of 0.990 for SJ-COF, YA-COF, and AA-COF), indicating that the iodine sorption by COFs followed the Langmuir model (SI, Section S7, Fig S17). Usually, the affinity constant (R_L) derived from the Langmuir model is employed to assess the isotherm's favorability and is represented by Eq. (5).
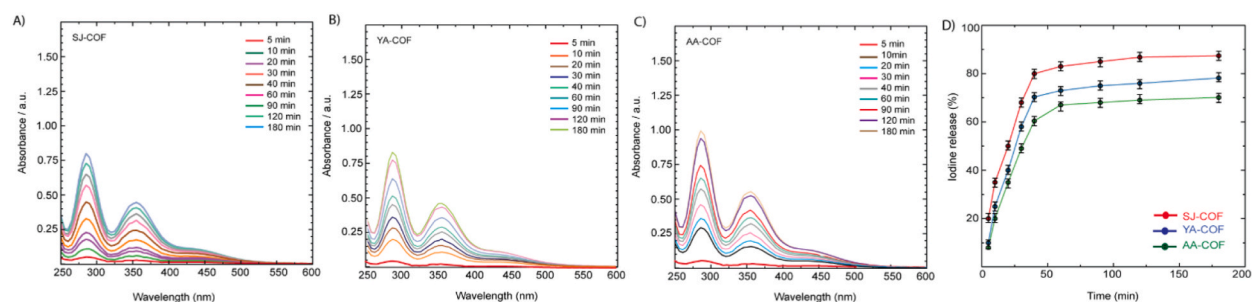
Fig. 5. Iodine Release Kinetics from COFs in Ethanol. Depicts the time-based evolution of UV–Vis absorption spectra for the release of iodine from SJ-COF (A), YA-COF (B), and AA-COF (C) in ethanol. Additionally, Panel D quantifies the rate of iodine release for each COF, providing a comparative analysis of their desorption dynamics. Error bars, representing standard deviations from three replicate measurements, affirm the precision of the data.
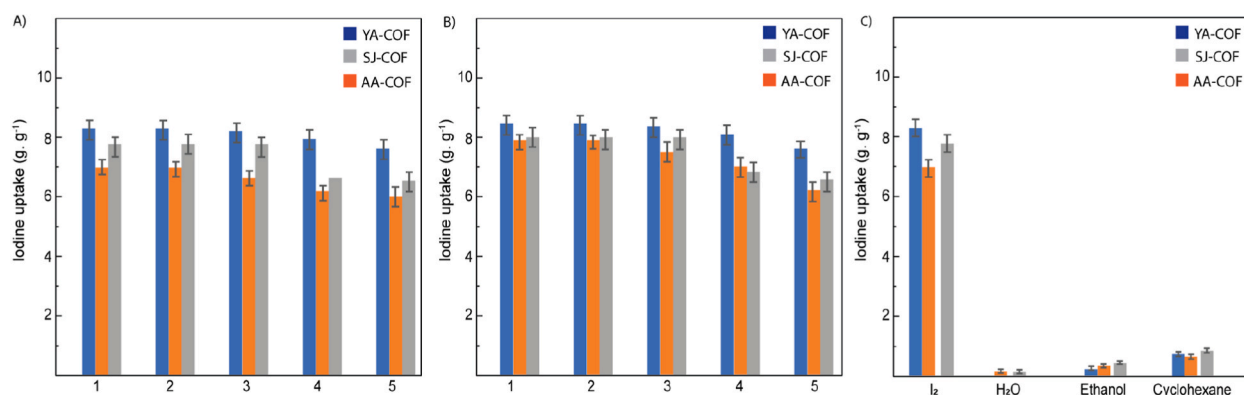
Fig. 6. COFs Reusability and Selectivity for Iodine Adsorption. Panel A and B show iodine adsorption from solution and gas phase over multiple cycles, proving COFs' effectiveness and reusability. Panel C highlights the selective adsorption of I_2 over H_2O, EtOH, and cyclohexane, demonstrating COFs' specificity. This underscores their potential in targeted pollutant removal and separation tasks.

$$R_L = \frac{1}{1 + k_L C_m} \tag{5}$$

The highest initial iodine concentration is given as C_m (mg/L). The value of R_L reveals the nature of the isotherm: when $R_L = 0$, the isotherm is believed to be irreversible; the isotherm is linear when $R_L = 1$, and it is unfavorable when $R_L > 1$ [27]. The R_L value for iodine in the present study was discovered to be 0.078, demonstrating the effectiveness of the adsorption process. According to the Langmuir model, monolayer adsorption takes place on a homogenous surface with uniform adsorption sites [28]. This suggests that the adsorption of iodine onto the COFs was significantly influenced by the development of monolayers. The maximum adsorption capacities (Q_m) for SJ-COF, YA-COF, and AA-COF in terms of iodine adsorption were determined by Langmuir isotherm analysis to be 960.15 mg/g, 895.20 mg/g, and 768.43 mg/g, respectively.

Iodine release. It is essential to ensure the reversibility of a possible iodine absorbent. In order to evaluate the iodine release from iodine-loaded SJ-COF, YA-COF, and AA-COF, we used a procedure that was identical to the iodine adsorption experiment. We also acquired the iodine-ethanol-dissolved standard curve (SI, Section S8, Fig S18). UV–vis spectroscopy was used to examine the iodine release from the iodine-loaded materials (Fig. 5A–C). Iodine was released from the channels as the black crystals were submerged in anhydrous ethanol, resulting in a progressive darkening to brown of the solution. The absorbance at 290 and 360 nm increased with the period of soaking. The iodine release curves of I_2@SJ-COF, I_2@YA-COF, and I_2@AA-COF exhibited a linear increasing trend, with 81.6%, 70.3%, and 60.4% of iodine being rapidly released within 40 min, and 87.4%, 78.3%, and 70.1% within 180 min (Fig. 5D). The behavior seen suggests that the SJ-COF, YA-COF, and AA-COF network and iodine have substantial interactions. The high affinity of iodine molecules for our COFs is further supported by the abundance of remaining iodine in the COFs. Furthermore, the recovered SJ-COF, YA-COF, and AA-COF in ethanol exhibit PXRD patterns that closely resemble those of the original COFs, confirming their stability and renewability.

Recovery and reusability. Adsorbents must be reusable in order to be used in real-world applications. The cyclic experiment was conducted to assess the three COFs' ability to recycle iodine capture. For the desorption experiment, the I_2@SJ-COF, I_2@YA-COF and I_2@AA-COF adsorbents were soaked in ethanol for 24 h after each run, centrifuged, dried at 85 °C for 12 h, and then COFs undertook another round after the initial gas phase adsorption to assess their suitability for further gas phase adsorption. For the removal of iodine
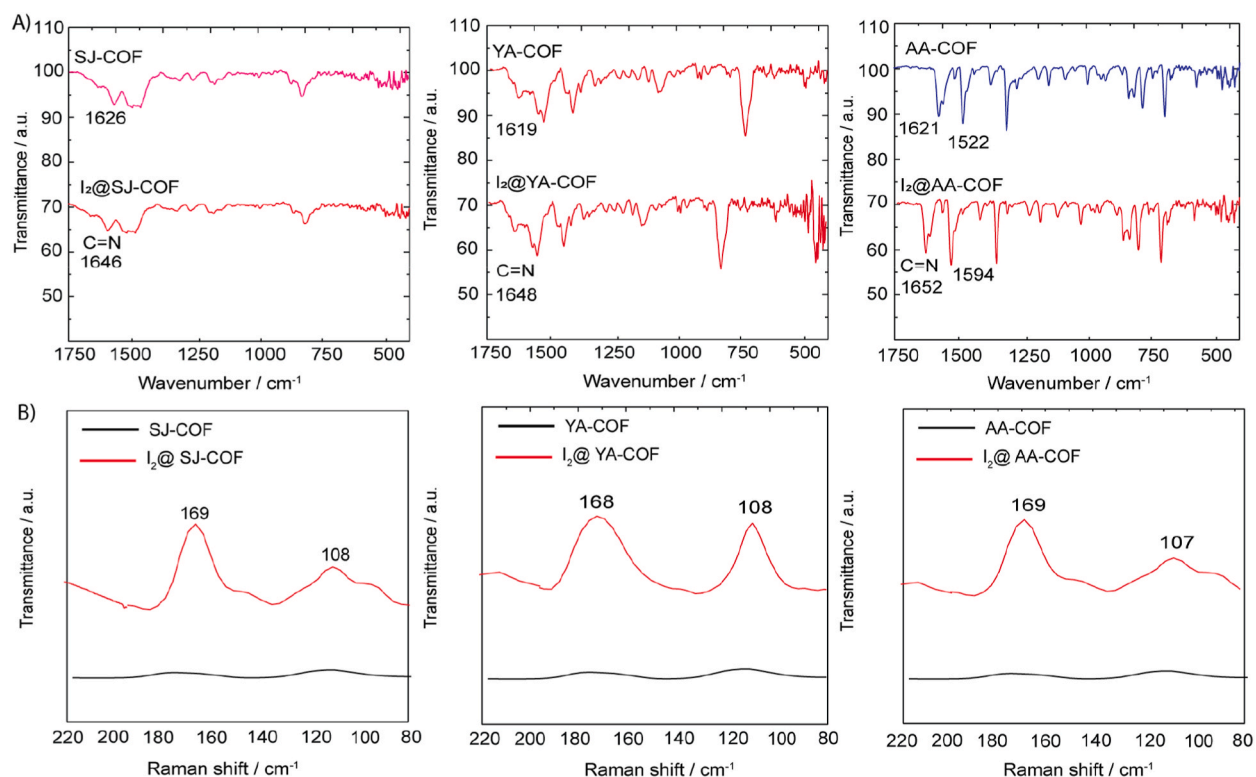
Fig. 7. FT-IR and Raman Spectra of COFs Before and After Iodine Adsorption. Illustrates the Fourier-transform infrared (FT-IR) spectra (A) and Raman spectra (B) of SJ-COF, YA-COF, AA-COF, as well as I$_2$@SJ-COF, I$_2$@YA-COF, and I$_2$@AA-COF. These analyses reveal the structural changes and interactions between COFs and iodine, critical for assessing adsorption efficacy and material integrity.

from the solution phase and after every cycle, the mixture was centrifuged to separate the adsorbent from the solution. The separated adsorbent was after that carefully washed with ethanol, and it was dried at 70 °C to ensure complete removal of the solvent and prepared for its next usage. Fig. 6A and B shows how COFs can be reused. Surprisingly, even after 5 repeated adsorptions and desorption cycles, the regenerated COFs maintained significant iodine sorption capabilities more than 6.7 g g^{-1}, highlighting its considerable adsorption potential. PXRD and FT-IR measurements verified that even after the fifth cycle, the regenerated COFs retained their crystallinity, even with discernible reductions (SI, Section S8, Fig S19–S21). The PXRD patterns of the regenerated COFs showed no change after cyclic application, proving that their crystallinity was not disrupted. The chemical stability of these COFs during the cyclic process was further confirmed by FT-IR spectroscopy. The similar finding was seen during the iodine removal from solution phase as well. The previously mentioned experimental findings along with earlier research show that the COFs iodine adsorbents have a number of outstanding attributes, including extraordinary capacity, quick kinetics, high adsorption stability, and great reusability. These characteristics make them very practical for radioiodine capture applications, and outstanding efficiency cycles indicate that these materials had oxidative iodine resistance even after prolonged exposure. A selective experiment utilizing iodine, water, ethanol, and cyclohexane as the adsorbents was carried out at temperature of 75 °C at atmospheric pressure, and the outcomes revealed that COFs had higher adsorption capacities toward iodine than toward water, ethanol, and cyclohexane (Fig. 6C), which was crucial for practical applications because COFs contain a lot of moisture in nuclear fuel reprocessing.

The iodine capture mechanism. To better comprehend the three COFs' iodine adsorption mechanisms, we conducted characterization using FT-IR and Raman spectroscopy. This allowed us to study the COFs both before and after the adsorption of iodine, which gave us important information on the underlying interactions between the COFs and iodine molecules. We first performed FT-IR spectroscopic investigation on I$_2$@SJ-COF, I$_2$@YA-COF, and I$_2$@AA-COF. The vibrational stretch of the –C=N group has shifted significantly when compared to the FT-IR spectra of the pristine COFs and the COFs that had been loaded with iodine. The peak changed for SJ-COF from 1646 c cm^{-1} to 1626 cm^{-1}, for YA-COF from 1648 cm^{-1}–1619 cm^{-1}, and for AA-COF from 1652 cm^{-1}–1621 cm^{-1} (Fig. 7A). The detected FT-IR shifts strongly implied the occurrence of a chemisorption process, likely arising from the presence of charge-transfer interactions among the nitrogen atom of the imine linkage in the COFs and iodine. Fig. 7B shows the findings of our Raman spectroscopy, which we used to further analyze the adsorbed iodine species. I$_2$@SJ-COF, I$_2$@YA-COF, and I$_2$@AA-COF all exhibited unique peaks at 108 and 169 cm^{-1}, 108 and 168 cm^{-1}, and 107 and 169 cm^{-1}, respectively, but pure COFs did not show any distinguishable peaks. The symmetric stretching vibration of polyiodide I$_3$ and polyiodide I$_5$ are responsible for the observed peaks, respectively. In accordance with the outcome, the three COFs' adsorbed iodine species exist as I$_2$ molecules as well as polyiodine anions. The data discussed above allow us to deduce the mechanism behind iodine vapor capture. Iodine vapor first undergoes
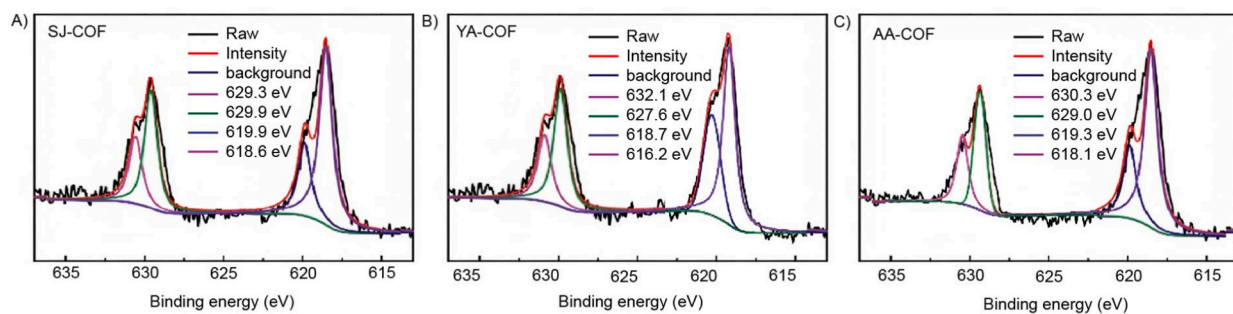
Fig. 8. XPS Analysis of Iodine-Loaded COFs: XPS of iodine for (A) SJ-COF, B) YA-COF and C) AA-COF after iodine uptake.
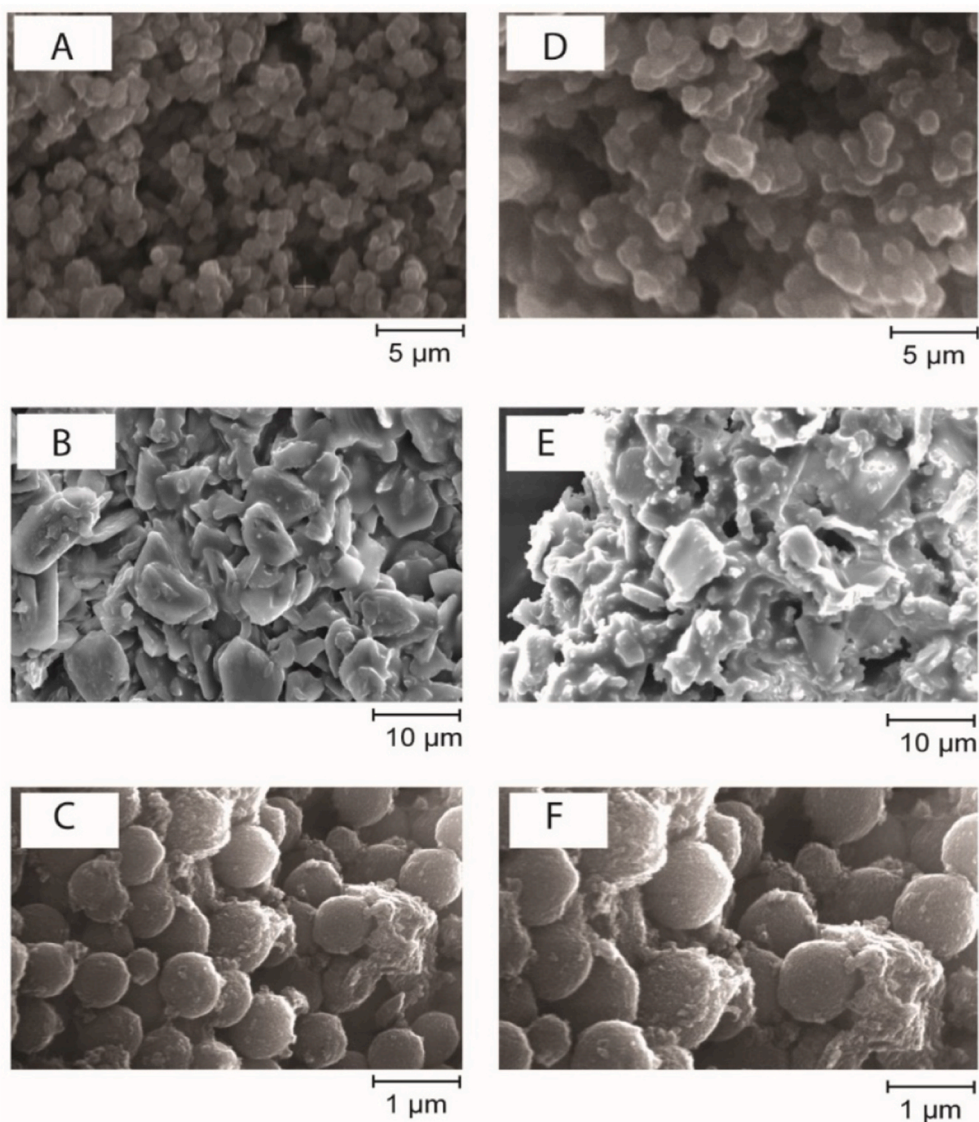
Fig. 9. SEM Analysis of COFs Before and After Iodine Absorption. This figure presents scanning electron microscopy (SEM) images showing the morphology of YA-COF (A), SJ-COF (B), and AA-COF (C) before iodine absorption, and the corresponding changes post-absorption in images YA-COF (D), SJ-COF (E), and AA-COF (F). These images visually demonstrate the impact of iodine uptake on the surface and structural characteristics of each COF, highlighting potential physical changes or stability post-adsorption, crucial for evaluating the suitability of these materials for iodine capture and storage applications.

physisorption and then is absorbed into the pores of COFs. The existence of chemisorption is then demonstrated by the formation of charge complexes with heteroatoms in the framework of the COFs. The extremely large iodine capture capacity is made possible by the combination of physisorption and chemisorption. These results support earlier research and offer important new understandings of the adsorption mechanism [29].

To examine the presence of iodine within the three COFs, we utilized X-ray photoelectron spectroscopy (XPS). In the figure, we observed distinct peaks situated at 629.3 eV and 617.3 eV for SJ-COF, 627.6 eV and 616.2 eV for YA-COF as well as 629.0 eV and 619.3 eV for AA-COF. These peaks correspond to the I $3d_{3/2}$ and I $3d_{5/2}$ orbitals of iodine molecules, suggesting that the captured iodine primarily exists in a molecular form. Additionally, we identified two more peaks at 629.9 eV and 618.6 eV for SJ-COF, 632.1 eV and 618.7 eV for YA-COF as well as 630.3 eV and 618.1 eV for AA-COF, indicative of the presence of polyiodine anions, including I_3^- and I_5^- [30] (Fig. 8A–C). Theoretical insights and literature evidence highlight the pivotal role of nitrogen (N) and sulfur (S) atoms within the functional groups of adsorbent materials in facilitating iodine adsorption. The electron-rich nature of N and S atoms is crucial for interactions with electron-deficient species like iodine (I_2), predominantly through charge-transfer complexes or electrostatic interactions. Specifically, the lone pair of electrons on N atoms and the capability of S atoms to act as soft Lewis bases enhance the adsorption capacity and selectivity of materials towards iodine. This theoretical framework is supported by existing studies that underscore the significance of N/S-containing functional groups as active sites for efficient iodine binding [31,32]. Although our study did not directly analyze the electronic environment of N and S atoms through XPS, the literature supports their expected contribution to the adsorption mechanism [33]. Future studies using XPS and other spectroscopic methods could empirically confirm these interactions, enhancing our grasp of iodine adsorption mechanisms. This aligns with our goal to further understand the role of N/S-functional groups, supported by theoretical and literature insights.

To achieve a comprehensive understanding of the adsorption mechanism of three COFs for iodine, we performed SEM analysis on both free COFs and iodine-adsorbed COFs. The SEM image illustrates that I_2@SJ-COF, I_2@YA-COF, and I_2@AA-COF mainly maintain their original loose porous networks, with only slight agglomeration (Fig. 9). YA-COF, AA-COF, and SJ-COF are significant candidates for iodine adsorption because of their distinctive characteristics and properties. These COFs have large surface areas and well-defined pore architectures, which promote enhanced iodine molecule adsorption by offering more active sites. Significantly, their strong thermal and chemical stability ensures that they are effective in capturing iodine even in harsh environments, which is an essential characteristic of adsorbents for radioactive waste. With exceptionally high iodine capture capacities and demonstrated selectivity coupled with multiple reuse cycles, these COFs exhibit a remarkable efficiency pivotal for nuclear waste management. Furthermore, the strong physical-chemical adsorption mechanism elucidates a potent interaction between the COFs and iodine molecules, elevating their adsorption efficacy to optimize the process.

4. Conclusion

In summary, a one-pot Schiff-base condensation process was used to create three COFs that are rich in heteroatoms. In addition to exhibiting outstanding performance in terms of thermal and chemical stability, the produced COFs also displayed great specific surface area. These benefits added together to provide the three COFs remarkable iodine sorption efficiency in both gaseous and liquid phases. With a large specific surface area, the YA-COF was able to collect more iodine in the vapor phase (8.52 g g^{-1}) than most previously reported adsorbents. The three COFs demonstrated extremely strong iodine adsorption capability with up to 80% removal efficiency in cyclohexane solution. As part of our investigation into the adsorption process, we reviewed relevant studies that showed iodine binding occurred by a combination of physisorption, chemisorption, as well as quick adsorption kinetics. Three COFs, in the meanwhile, have demonstrated strong recycling usage capabilities and can be recycled and utilized at least five times. This research offers a fresh concept for creating practical COFs that can capture iodine. Based on these findings, it is clear that functionalized COF materials have enormous potential for effectively removing iodine, especially during environmental emergencies and incidents that require for quick response to harmful substances. Our research serves as an initial step in demonstrating the adsorption capabilities of these COFs and their potential for addressing iodine contamination. Further investigation and collaboration with experts in the relevant fields will be necessary to assess their applicability on a larger scale.

CRediT authorship contribution statement

Shaikha S. AlNeyadi: Writing – original draft, Writing – review & editing, Visualization, Validation, Supervision, Software, Resources, Project administration, Methodology, Investigation, Funding acquisition, Formal analysis, Data curation, Conceptualization. **Mohammed T. Alhassani:** Methodology, Investigation, Data curation, Conceptualization. **Ali S. Aleissaee:** Methodology. **Sultan. J:** Methodology. **Abdullah H. Khalaf:** Methodology. **Abdulrahman A. Alteneij:** Methodology. **Yaser Y. Alyaarbi:** Methodology.

Declaration of competing interest

The authors declare the following financial interests/personal relationships which may be considered as potential competing interests:Shaikha alneyadi reports financial support was provided by United Arab Emirates University. SHAIKHA ALNEYADI reports a relationship with UAE University Department of Chemistry that includes: employment and funding grants.

Acknowledgements

Appendix A. Supplementary data

Supplementary data to this article can be found online at https://doi.org/10.1016/j.heliyon.2024.e25921.

References

[1] R.C. Ewing, F.N. von Hippel, Energy. Nuclear waste management in the United States–starting over, Science 325 (5937) (2009) 151–152, https://doi.org/10.1126/science.1174594.

[2] M.I. Ojovan, W.E. Lee, S.N. Kalmykov, An Introduction to Nuclear Waste Immobilisation, Elsevier, 2019, https://doi.org/10.1016/B978-0-08-102702-8.00013-3.

[3] D. Taylor, The radiotoxicology of iodine, J. Radioanal. Nucl. Chem. 65 (1–2) (1981) 195–208, https://doi.org/10.1007/bf02516104.

[4] J.E. Ten Hoeve, M.Z. Jacobson, Worldwide health effects of the Fukushima Daiichi nuclear accident, Energy Environ. Sci. 5 (9) (2012) 8743–8757, https://doi.org/10.1039/C2EE22019A.

[5] G. Mushkacheva, et al., Thyroid abnormalities associated with protracted childhood exposure to 131I from atmospheric emissions from the Mayak weapons facility in Russia, Radiat. Res. 166 (5) (2006) 715–722, https://doi.org/10.1667/RR0410.1.

[6] B. Liu, et al., High efficient adsorption and storage of iodine on S, N co-doped graphene aerogel, J. Hazard Mater. 373 (2019) 705–715, https://doi.org/10.1016/j.jhazmat.2019.04.005.

[7] Y.A.B. Neolaka, et al., Potential of activated carbon from various sources as a low-cost adsorbent to remove heavy metals and synthetic dyes, Results in Chemistry 5 (2023) 100711, https://doi.org/10.1016/j.rechem.2023.100711.

[8] Y.-T. Zhang, et al., Enhancing methane production from algae anaerobic digestion using diatomite, J. Clean. Prod. 315 (2021) 128138, https://doi.org/10.1016/j.jclepro.2021.128138.

[9] Z. Qiu, et al., Enhanced cellulosic d-lactic acid production from sugarcane bagasse by pre-fermentation of water-soluble carbohydrates before acid pretreatment, Bioresour. Technol. 368 (2023) 128324, https://doi.org/10.1016/j.biortech.2023.128324.

[10] C. Wei, et al., Ozonation in water treatment: the generation, basic properties of ozone and its practical application, Rev. Chem. Eng. 33 (1) (2017) 49–89, https://doi.org/10.1515/revce-2016-0008.

[11] J. Wang, L.E. Xu, Advanced oxidation processes for Wastewater treatment: formation of Hydroxyl Radical and application, Crit. Rev. Environ. Sci. Technol. 42 (2012) 251–325, https://doi.org/10.1080/10643389.2010.507698.

[12] D. Elder, Pharmaceutical applications of ion-exchange Resins, J. Chem. Educ. 82 (2005), https://doi.org/10.1021/ed082p575.

[13] P. Kumar, et al., Metal organic frameworks (MOFs): current trends and challenges in control and management of air quality, Kor. J. Chem. Eng. 36 (2019) 1839–1853, https://doi.org/10.1007/s11814-019-0378-8.

[14] Y. Tian, G. Zhu, Porous aromatic frameworks (PAFs), Chem. Rev. 120 (16) (2020) 8934–8986, https://doi.org/10.1021/acs.chemrev.9b00687.

[15] K. Geng, et al., Covalent organic frameworks: design, synthesis, and Functions, Chem. Rev. 120 (16) (2020) 8814–8933, https://doi.org/10.1021/acs.chemrev.9b00550.

[16] Y. Yang, et al., Molecular iodine capture by covalent organic frameworks, Molecules 27 (24) (2022) 9045, https://doi.org/10.3390/molecules27249045.

[17] J. Yang, et al., Magnetic covalent organic framework composites for Wastewater remediation, Small 19 (37) (2023) 2301044, https://doi.org/10.1002/smll.202301044.

[18] D. Zhu, et al., Pure crystalline covalent organic framework Aerogels, Chem. Mater. 33 (11) (2021) 4216–4224, https://doi.org/10.1021/acs.chemmater.1c01122.

[19] M. Zhou, et al., Highly conjugated two-dimensional covalent organic frameworks for efficient iodine uptake, Chem.–Asian J. 17 (15) (2022) e202200358, https://doi.org/10.1002/asia.202200358.

[20] Z.-J. Yin, et al., Ultrahigh volatile iodine uptake by hollow microspheres formed from a heteropore covalent organic framework, Chem. Commun. 53 (53) (2017) 7266–7269, https://doi.org/10.1039/C7CC01045A.

[21] K.W. Chapman, P.J. Chupas, T.M. Nenoff, Radioactive iodine capture in silver-containing mordenites through nanoscale silver iodide formation, J. Am. Chem. Soc. 132 (26) (2010) 8897–8899, https://doi.org/10.1021/ja103110y.

[22] D.F. Sava, et al., Capture of volatile iodine, a gaseous fission product, by zeolitic imidazolate framework-8, J. Am. Chem. Soc. 133 (32) (2011) 12398–12401, https://doi.org/10.1021/ja204757x.

[23] Z. Yan, et al., Highly efficient Enrichment of volatile iodine by charged porous aromatic frameworks with three sorption sites, Angew. Chem. Int. Ed. 54 (43) (2015) 12733–12737, https://doi.org/10.1002/anie.201503362.

[24] M.B. Schaffler, et al., Osteocytes: master orchestrators of bone, Calcif. Tissue Int. 94 (1) (2014) 5–24, https://doi.org/10.1007/s00223-013-9790-y.

[25] D.K.L. Harijan, et al., Radioactive iodine capture and storage from water using magnetite nanoparticles encapsulated in polypyrrole, J. Hazard Mater. 344 (2018) 576–584, https://doi.org/10.1016/j.jhazmat.2017.10.065.

[26] H. Li, X. Ding, B.-H. Han, Porous azo-bridged porphyrin–phthalocyanine network with high iodine capture capability, Chem. Eur J. 22 (33) (2016) 11863–11868, https://doi.org/10.1002/chem.20160.

[27] T. Li, F. He, Y. Dai, Prussian blue analog caged in chitosan surface-decorated carbon nanotubes for removal cesium and strontium, J. Radioanal. Nucl. Chem. 310 (3) (2016) 1139–1145, https://doi.org/10.1007/s10967-016-4980-5.

[28] W. Zhang, et al., Cross-linked chitosan microspheres: an efficient and eco-friendly adsorbent for iodide removal from waste water, Carbohydr. Polym. 209 (2019) 215–222, https://doi.org/10.1016/j.carbpol.2019.01.032.

[29] Z. Yan, B. Chen, T. He, R. Krishna, W. Zhou, Highly efficient Enrichment of volatile iodine by charged porous aromatic frameworks with three sorption sites, Angew. Chem. Int. Ed. 54 (43) (2015) 12733–12737, https://doi.org/10.1002/anie.201503362.

[30] S.L. Hsu, et al., Highly conducting iodine derivatives of polyacetylene: Raman, XPS and x-ray diffraction studies, J. Chem. Phys. 69 (1) (2008) 106–111, https://doi.org/10.1063/1.436393.

[31] B. Petrovic, M. Gorbounov, S. Masoudi Soltani, Impact of surface functional groups and their introduction methods on the mechanisms of CO2 adsorption on porous Carbonaceous adsorbents, Carbon Capture Science & Technology 3 (2022) 100045, https://doi.org/10.1016/j.ccst.2022.100045.

[32] N. Kasera, P. Kolar, S.G. Hall, Nitrogen-doped biochars as adsorbents for mitigation of heavy metals and organics from water: a review, Biochar 4 (1) (2022) 17, https://doi.org/10.1007/s42773-022-00145-2.

[33] X. Liu, et al., Orderly porous covalent organic frameworks-based materials: superior adsorbents for pollutants removal from aqueous solutions, Innovation 2 (1) (2021) 100076, https://doi.org/10.1016/j.xinn.2021.100076.